COMMUNICATION

Nanoporous Metal Membranes with Bicontinuous Morphology from Recyclable Block-Copolymer Templates

By *Yong Wang,* Changcheng He, Weihong Xing,* Fengbin Li, Ling Tong, Zhiquan Chen, Xingzhi Liao,* and *Martin Steinhart**

Nanoporous scaffolds have been exploited for separation,[1–3] catalysis,[4] optical coating,[5] tissue engineering,[6] and sensing.[7] However, the preparation of nanoporous metal membranes or metal monoliths with bicontinuous morphologies, which may show significantly enhanced accessibility from the ambiance and likewise significantly enhanced mass transport rates, is still challenging. Synthetic approaches to generate continuous nanopore systems are predominantly based on spinodal decomposition or on the use of structure-directing soft templates. Spinodal decomposition in inorganic glasses[8] and metal alloys[9] yields well-defined pore sizes but requires high-temperature treatments and must be combined with the etching of one component. Ordered bicontinuous nanoporous materials can be synthesized by sol–gel chemistry along with calcination of sacrificial structure-directing soft templates,[10,11] by selective degradation of one of the blocks in block copolymers (BCPs),[12–14] and by microemulsion templating combined with crosslinking of the polymeric scaffold.[15] However, in all synthetic approaches mentioned so far either components of mixtures or structure-directing soft templates are consumed. Further, nondestructive preparation methods, such as nonsolvent-induced phase separation in the presence of BCPs[2,3] and liquid/liquid phase separation in polymeric solutions,[16,17] typically yield bicontinuous porous membranes lacking a high degree of structural uniformity. Hence, it has remained challenging to produce materials containing well-defined continuous pore systems characterized by narrow pore-size distributions centering on a few tens of nanometers in a nondestructive way.

Here, we report the preparation of metal membranes characterized by easily accessible, continuous nanopore systems with well-defined, uniform pore sizes by nondestructive replication of nanoporous polymeric membranes with likewise bicontinuous morphologies. The nanoporous polymeric membranes consisted of recoverable asymmetric BCPs and were generated by selectively swelling the minority component of the BCP accompanied by reconstruction of the domains consisting of the glassy majority component. Swelling-induced surface reconstruction in thin BCP films with thicknesses corresponding to the characteristic periods of the BCPs has been studied intensively.[18–28] Moreover, swelling minority domains in BCP nanorods resulted in the intermediate formation of meshlike structures that eventually transformed into strings of micelles.[29] However, little effort has been devoted to explore swelling minority domains in bulklike BCP specimens with dimensions exceeding the BCP period by at least one order of magnitude to access membrane configurations characterized by continuous nanopore systems. As displayed in Figure 1, initially separated spherical or cylindrical domains consisting of the minority component of an asymmetric BCP are swollen with a selective solvent (panel a). As its volume increases upon uptake of solvent, the minority component pierces through the glassy majority component, and a bicontinuous morphology evolves (panel b). Pushed outward by the solvent, the swelling minority component forms a continuous layer at the membrane surface that is connected to the continuous network of swollen minority domains within the membrane. As the solvent evaporates, the swollen minority blocks collapse, but the nanoscopic morphology of the partially swollen BCP membrane is fixated by the rigid, continuous scaffold formed by the glassy majority component. Thus, nanopores with walls consisting of the collapsed blocks form in the place of the swollen minority domains (panel c). The collapse of the surface layer consisting of the swellable minority
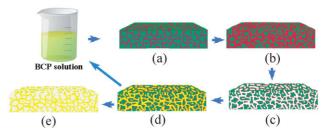
[*] Prof. Y. Wang, Prof. W. Xing, F. Li, L. Tong, Z. Chen, X. Liao, X. Liao
State Key Laboratory of Materials-Oriented Chemical Engineering, College of Chemistry and
Chemical Engineering, Nanjing University of Technology
Nanjing 210009, Jiangsu (P. R. China)
E-mail: yongwang@njut.edu.cn; xingwh@njut.edu.cn
Fax: 0086-25-8317-2292
Dr. C. He
College of Chemistry, Beijing Normal University
Beijing, 100875 (P. R. China)
Prof. M. Steinhart
Institute for Chemistry, University of Osnabrück
Barbarastraße 7, D-49069 Osnabrück (Germany)
E-mail: martin.steinhart@uni-osnabrueck.de
Fax: 0049-541-969-3324

Figure 1. Nondestructive preparation of nanoporous metal membranes with bicontinuous morphology by replication of nanoporous membranes consisting of recyclable asymmetric BCPs (green, glassy matrix of the BCP; red, swellable component of the BCP; yellow, deposited metal). a) Unswollen BCP. b) Partially swollen BCP after morphology reconstruction. c) Nanoporous BCP membrane after collapse of the swollen domains caused by solvent evaporation and d) after deposition of the metal into the pores. e) nanoporous metal membrane after recovery of the BCP by extraction.

component on top of the BCP membrane leads to the formation of an open nanopore system exposed to the ambience. In the same way, openings of the nanopore system also form at the underside of the BCP membrane attached to an underlying substrate if the swelling minority component wets the substrate surface prior to its collapse. As a result, nanoporous BCP membranes with open, easily accessible nanopore systems are obtained. If the substrate is conductive, metals can be deposited into the continuous nanopore system by electrodeposition[30] (panel d). Finally, the BCP can be extracted. Reverse replicas of the nanoporous BCP membranes are thus obtained, whereas the BCP can be recovered and reused (panel e).

Polystyrene-*block*-poly(2-vinyl pyridine) [M_n (polystyrene, PS) $= 50000\,g\,mol^{-1}$; M_n (poly(2-vinyl pyridine), P2VP) $= 16500\,g\,mol^{-1}$; bulk period $\sim$42 nm; hereafter denoted PS_50-*b*-P2VP_17], an amphiphilic BCP that forms P2VP cylinders surrounded by a PS matrix, was swollen in ethanol, a solvent selective to P2VP, at 60 °C for different periods of time. Figure 2a–d shows scanning electron microscopy (SEM) images of a PS_50-*b*-P2VP_17 membrane prepared by spin-coating solutions of 3 wt% BCP in tetrahydrofuran onto Si wafers after swelling and evaporation of the ethanol. The $\sim$300-nm-thick, as-deposited PS_50-*b*-P2VP_17 film contained apparently in-plane but randomly oriented P2VP cylinders seen as darker areas in the PS matrix with an apparent spacing of $\sim$42 nm (Fig. S1 in the Supporting Information). After swelling for 10 min, nanopores formed, while the cylindrical morphology with an apparent period of $\sim$48 nm was still intact (Fig. 2a). After swelling for 1 h, a morphology intermediate between the disordered-cylindrical and bicontinuous structure types emerged (Fig. 2b). After 4 h, a completely developed bicontinuous morphology is seen (Fig. 2c), which slightly coarsened after swelling for eleven more hours (Fig. 2d). While the pore diameter increased from $\sim$25 nm after swelling for 1 h to $\sim$40 nm after swelling for 15 h, the polymeric pore walls had, independent of the swelling time, a constant thickness of $\sim$35 nm. The network of nanopores obtained after swelling for 15 h is uniform over the entire membrane thickness, which increased from initially $\sim$300 to $\sim$1000 nm (Fig. 2e). Both the top surfaces and the undersides of the swollen PS_50-*b*-P2VP_17 membranes were characterized by identical, open nanoporous structures (Fig. S2). PS_50-*b*-P2VP_17 membranes swollen for 15 h were further characterized by measuring nitrogen adsorption isotherms (Fig. 2f). Brunauer–Emmett–Teller analysis revealed a type-IV isotherm as well as a specific surface area of $42\,m^2\,g^{-1}$ and confirmed the nanoporous nature of the PS-*b*-P2VP membrane. The relatively narrow pore-size distribution (Fig. 2f, inset) with a full width at half maximum of $\sim$35 nm was determined by the Barrett–Joyner–Halenda method and is centering on a value of $\sim$38 nm. While the specific surface of the PS_50-*b*-P2VP_17 membranes is smaller than that of mesoporous materials with pore diameters in the sub-10-nm range, the results obtained here match those reported by Zhou et al. for mesoporous polymeric specimens prepared by microemulsion templating.[15]

Bicontinuous sponge-like structures were also obtained by swelling PS_28-*b*-P2VP_4 (M_n (PS) $=27\,700\,g/mol$; M_n (P2VP) $=4300\,g/mol$; bulk period $\sim$26 nm), a BCP containing P2VP spheres in a PS matrix, in ethanol at 60 °C and subsequent evaporation of the ethanol. Cross-sectional views of
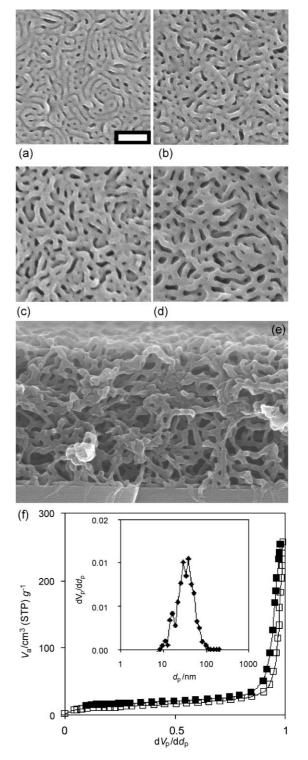

Figure 2. SEM images and adsorption isotherms of PS_50-*b*-P2VP_17 membranes at different stages of swelling with ethanol at 60 °C. a–d) Top views after swelling times of a) 10 min, b) 1 h, c) 4 h, and d) 15 h. e) Cross-sectional view of a PS_50-*b*-P2VP_17 membrane after swelling for 15 h. Panels (a–e) have the same magnification. The scale bar in (a) corresponds to 200 nm. f) Nitrogen adsorption isotherm of a nanoporous PS_50-*b*-P2VP_17 membrane swollen for 15 h (adsorption, open squares; desorption, solid squares). The inset shows the pore size distribution derived from desorption data.

PS_28-*b*-P2VP_4 membranes swollen for 10 min, 4 h and 15 h are shown in Figure 3a–c. After swelling for 10 minutes, the membrane apparently contained no pores (Figure 3a). After swelling for 1h a bicontinuous morphology was completely developed (not shown). The pore diameter amounted to ~20 nm after swelling for 4 h (Figure 3b) and increased only moderately to ~30 nm after swelling for 15 h (Figure 3c), while the thickness of the polymeric pore walls of ~33 nm remained constant. After swelling for 10 minutes, the PS_28-*b*-P2VP_4 membranes had a thickness of ~530 nm that increased to ~650 nm after swelling for 4h and to ~730 nm after swelling for 15 h. Figure 3d shows a top view of the nanoporous surface of a PS_28-*b*-P2VP_4 membrane swollen 15 h.

A broad range of asymmetric PS-*b*-P2VP BCPs shows a robust tendency to form bicontinuous morphologies upon selective swelling of P2VP. However, swelling slightly asymmetric lamellar PS_26-*b*-P2VP_24 $[M_n(PS) = 25\ 5000\ \text{g mol}^{-1};\ M_n(\text{P2VP}) = 23\ 5000\ \text{g mol}^{-1}]$ with ethanol heated to 60 °C resulted in the breakup of the PS domains into isolated entities already after 10 min (Fig. S3a), and swelling for 15 h yielded arrays of discrete micelles with a diameter of ~36 nm and a period of ~43 nm (Fig. S3b). Thus, intermediate stages characterized by bicontinuous morphologies only occur if the initial volume fraction of the minority component lies below a threshold value in between of the values characteristic of lamellar and cylindrical morphologies.

Bicontinuous morphologies represent transient non-equilibrium stages in the swelling-induced transformation of bulk asymmetric PS-*b*-P2VP into PS-*b*-P2VP micelles in ethanolic solutions.
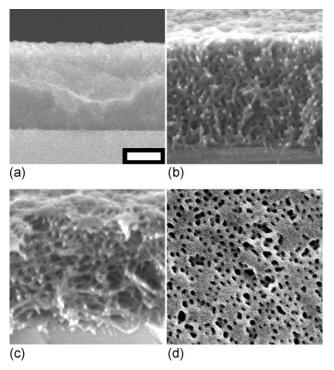

Figure 3. SEM images of PS-*b*-P2VP membranes at different stages of swelling with ethanol at 60 °C. (a–c) Cross-sectional views of membranes consisting of the sphere-forming BCP PS_28-*b*-P2VP_4 after swelling for a) 10 minutes, b) 4 h, and c) 15 h. d) Top view of the surface of a PS_28-*b*-P2VP_4 membrane after swelling for 15 h. Panels (a–d) have the same magnification. The scale bar in (a) corresponds to 200 nm.

The Flory–Huggins interaction parameter of ethanol and P2VP was reported to be 0.499, a value typical of good solvent/polymer systems.[31] Ethanol readily diffuses through glassy PS and can swell even isolated P2VP domains surrounded by PS within minutes.[32] The highly uniform morphology across the PS-*b*-P2VP membranes rules out diffusion-controlled kinetics accompanied by morphology gradients. Swelling-induced morphology reconstruction involves plastic deformation of the glassy PS scaffold to dissipate the stress caused by the osmotic pressure of the solvent ethanol inside the PS-*b*-P2VP membranes. The P2VP blocks attached to the glassy PS scaffold expand because of the occurrence of excluded-volume forces. However, at some point in the swelling process, entropic restoring forces in the P2VP blocks will balance the excluded volume forces, and further uptake of ethanol is impeded. Then, the reduction of the internal interfacial area remains the only driving force for morphology reconstruction, which should correspondingly be slowed down. If minority blocks in asymmetric BCPs are swollen with non-ionic good solvents, such a kinetic transition apparently occurs at stages of the swelling process characterized by bicontinuous morphologies, which can conveniently be conserved by evaporation of the swelling agent from the partially swollen membranes. This evaporation process is characterized by the following features: i) The rigid, glassy PS scaffold fixates the morphology, and no delicate aging processes, as in the case of BCP-templated sol–gel chemistry, are required. ii) The expanded P2VP chains at the drying front collapse because of entropic relaxation. Therefore, ethanol can quickly migrate out of the PS-*b*-P2VP membranes through the pores thus formed. It should be noted that acidic swelling agents protonating the P2VP accelerate morphology reconstruction significantly because of the electrostatic repulsion between the charged P2VP chains. For example, exposure to acetic acid at 60° converts PS_50-*b*-P2VP_17 membranes into arrays of separated micelles already after 10 min (Fig. S4).

We prepared a gold replica of a 1000-nm-thick nanoporous PS_50-*b*-P2VP_17 membrane, which was attached to an underlying platinum-coated silicon substrate and swollen for 15 h by electrodeposition in a standard three-electrode electrochemical cell. To avoid overgrowth, we adjusted the plating time in such a way that the PS_50-*b*-P2VP_17 membrane was only partially filled up to a height of ~400 nm. The BCP was then removed by extraction with dimethylformamide (DMF) for 12 h at room temperature. Hence, a nanoporous gold membrane containing pores with a diameter of ~35 nm, separated by ~70-nm-thick walls was obtained (Fig. 4a). Its morphology was uniform over its entire thickness (Fig. 4b). The representative energy-dispersive EDX spectrum of the Au membrane shown in Figure 4c contains pronounced Au M_α and M_β peaks at ~2.1 keV and a weak Si K_α peak at ~1.7 keV originating from the substrate. Strikingly, only very weak carbon K_α and K_β peaks at ~0.27 keV appear, indicating the absence of carbon apart from residual contaminations. By spreading the DMF solution containing the extracted BCP on a Si wafer and evaporation of the solvent, a BCP film was obtained that could again be converted into a nanoporous membrane by reswelling in ethanol, as described above (Fig. S5). Tentative experiments revealed that other metals, such as platinum, can be deposited into swollen PS_50-*b*-P2VP_17 membranes also (Fig. S6).

In conclusion, the nondestructive preparation of bicontinuous, nanoporous metal membranes by replication of asymmetric
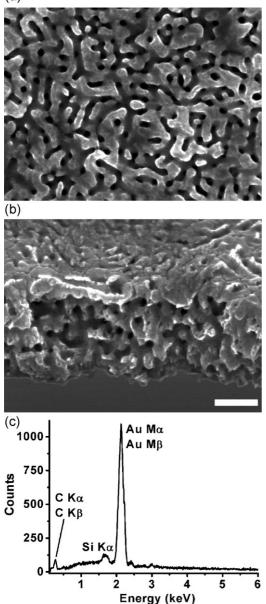
Materials
Views
www.MaterialsViews.com

ADVANCED
MATERIALS
www.advmat.de

COMMUNICATION

Figure 4. SEM images and EDX spectrum of a gold replica of a PS_50-*b*-P2VP_17 membrane obtained by swelling for 15 h in ethanol at 60 °C after extraction of the BCP. a) Top surface and b) bird's eye view (tilt angle 45°) of a cross-section. Panels (a) and (b) have the same magnification. The scale bar in (b) corresponds to 200 nm. c) Representative EDX spectrum.

such as galvanic displacement reactions[28] and atomic layer deposition,[33] can also be applied. Since the BCP is not consumed by partial degradation, calcination, or crosslinking, it can be recovered by extraction from the nanoporous metal scaffold. Thus, metal replicas of the BCP membranes containing likewise open and continuous nanopore systems are obtained.

Experimental

Preparation of PS-b-P2VP Membranes: PS_50-*b*-P2VP_17 [M_n (PS) = 50000 g mol^{-1}; M_n (P2VP) = 16500 g mol^{-1}; M_w/M_n (PS-*b*-P2VP) = 1.09], PS_28-*b*-P2VP_4 [M_n (PS) = 27700 g mol^{-1}; M_n (P2VP) = 4300 g mol^{-1}; M_w/M_n (PS-*b*-P2VP) = 1.04], and PS_26-*b*-P2VP_24 [M_n(PS) = 25500 g mol^{-1}; M_n(P2VP) = 23500 g mol^{-1}; M_w/M_n (PS-*b*-P2VP) = 1.05] were purchased from Polymer Source Inc., Canada. Solutions of 3 wt% BCP in tetrahydrofuran (THF) were spin-coated onto cleaned Si substrates at 2000 rpm for 60 s.

Preparation of Nanoporous Metal Membranes: Details of the electrodeposition process are described elsewhere [34,35]. Briefly, a commercially available plating solution (Orotemp; Technic Inc.; major component $KAu(CN)_2$) was used for the electrodepostion of gold. Deposition for 90 s yielded a ∼400-nm-thick Au layer. Electrodeposition of platinum was carried out in a similar way while using 0.01 mol L^{-1} aqueous K_2PtCl_6 solution as the Pt precursor.

Characterization: SEM images were taken on a Hitachi S4800 field-emission SEM operated at 10 keV. Polymeric samples were sputter-coated with a thin layer of gold/palladium alloy. For energy-dispersive X-ray spectroscopy (EDX), an EDX system Bruker AXS was used. Nitrogen adsorption–desorption isotherms were obtained at 77 K using an OMNISORP 100CX analyzer. Before the measurements, the PS-*b*-P2VP membranes were outgassed at 50 °C in vacuum for 5 h.

Note added in proof: On the authors' request the SEM images of Figures 2e and 3a–d were replaced with new ones that show different views of the same samples during the galley proofs stage. In addition, the captions to Figure 2 and 3 and the paragraph on page 3, column 1, lines 6–21 were reworded. These amendments were requested to further clarify and support the main statements presented in the manuscript.

amphiphilic block copolymer membranes was reported. Initially spherical or cylindrical morphologies of the BCPs were converted into bicontinuous morphologies by selective swelling of the minority domains. Evaporation of the solvent resulted in the collapse of the swollen domains, and BCP membranes containing open, continuous nanopore systems easily accessible from outside with well-defined pore sizes formed. The BCP membranes were used as recyclable molds in the electrodeposition of metals, but it is straightforward that other deposition methods,

[1] L. Chen, W. A. Phillip, E. L. Cussler, M. A. Hillmyer, *J. Am. Chem. Soc.* **2007**, *129*, 13786.

[2] K.-V. Peinemann, V. Abetz, P. F. W. Simon, *Nat. Mater.* **2007**, *6*, 992.

[3] F. Schacher, M. Ulbricht, A. H. E. Müller, *Adv. Funct. Mater.* **2009**, *19*, 1040.

[4] N. B. McKeown, P. M. Budd, *Chem. Soc. Rev.* **2006**, *35*, 675.

[5] W. Joo, M. S. Park, J. K. Kim, *Langmuir* **2006**, *22*, 7960.

[6] J. Norman, T. Desai, *Ann. Biomed. Eng.* **2006**, *34*, 89.

[7] H. Uehara, M. Kakiage, M. Sekiya, D. Sakuma, T. Yamonobe, N. Takano, A. Barraud, E. Meurville, P. Ryser, *ACS Nano* **2009**, *3*, 924.

[8] D. Enke, F. Janowski, W. Schwieger, *Microporous Mesoporous Mater.* **2003**, *60*, 19.

[9] J. Erlebacher, M. J. Aziz, A. Karma, N. Dimitrov, K. Sieradzki, *Nature* **2001**, *410*, 450.

[10] K. M. McGrath, D. M. Dabbs, N. Yao, I. A. Aksay, S. M. Gruner, *Science* **1997**, *277*, 552.

[11] V. Z.-H. Chan, J. Hoffman, V. Y. Lee, H. Iatrou, A. Avgeropoulos, N. Hadjichristidis, R. D. Miller, E. L. Thomas, *Science* **1999**, *286*, 1716.

[12] M. A. Hillmyer, *Adv. Polym. Sci.* **2005**, *190*, 137, and references therein.

[13] D. A. Olson, L. Chen, M. A. Hillmyer, *Chem. Mater.* **2008**, *20*, 869, and references therein.

[14] S. Ndoni, L. Li, L. Schulte, P. P. Szewezykowski, T. W. Hansen, F. X. Guo, R. H. Berg, M. E. Vigild, *Macromolecules* **2009**, *42*, 3877.

[15] N. Zhou, F. S. Bates, T. P. Lodge, *Nano. Lett.* **2006**, *6*, 2354.

[16] J. Arnauts, H. Berghmans, *Polym. Commun.* **1987**, *28*, 66.

[17] R. M. Hikmet, S. Callister, A. Keller, *Polymer* **1988**, *29*, 1378.

[18] Y. Boontongkong, R. E. Cohen, *Macromolecules* **2002**, *35*, 3647.

[19] T. Xu, J. Stevens, J. Villa, J. T. Goldbach, K. W. Guarini, C. T. Black, C. J. Hawker, T. P. Russell, *Adv. Funct. Mater.* **2003**, *13*, 698.

[20] C. Xu, B. B. Wayland, M. Fryd, K. I. Winey, R. J. Composto, *Macromolecules* **2006**, *39*, 6063.

[21] A. Sidorenko, I. Tokarev, S. Minko, M. Stamm, *J. Am. Chem. Soc.* **2003**, *125*, 12211.

[22] X. Li, S. J. Tian, Y. Ping, D. H. Kim, W. Knoll, *Langmuir* **2005**, *21*, 9393.

[23] Y. Cong, Z. Zhang, J. Fu, J. Li, Y. Han, *Polymer* **2005**, *46*, 5377.

[24] J. Chai, D. Wang, X. Fan, J. M. Buriak, *Nat. Nanotechnol.* **2007**, *2*, 500.

[25] S. Park, J. Y. Wang, B. Kim, J. Xu, T. P. Russell, *ACS Nano* **2008**, *2*, 766.

[26] Y. Wang, J. Q. Liu, S. Christiansen, D. H. Kim, U. Gösele, M. Steinhart, *Nano Lett.* **2008**, *8*, 3993.

[27] Y. Wang, M. Becker, L. Wang, J. Liu, R. Scholz, J. Peng, U. Gösele, S. H. Christiansen, D. H. Kim, M. Steinhart, *Nano Lett.* **2009**, *9*, 2384.

[28] M. Aizawa, J. M. Buriak, *J. Am. Chem. Soc.* **2005**, *127*, 8932.

[29] Y. Wang, U. Gösele, M. Steinhart, *Nano Lett.* **2008**, *8*, 3548.

[30] M. J. Tierney, C. R. Martin, *J. Phys. Chem.* **1989**, *93*, 2878.

[31] H. Akin, N. Hasirci, *J. Appl. Polym. Sci.* **1992**, *46*, 1307.

[32] Y. Wang, Y. Qin, A. Berger, E. Yau, C. He, L. Zhang, U. Gösele, M. Knez, M. Steinhart, *Adv. Mater.* **2009**, *21*, 2763.

[33] M. Knez, K. Nielsch, L. Niinistö, *Adv. Mater.* **2007**, *19*, 3425.

[34] L. Liu, W. Lee, Z. Huang, R. Scholz, U. Gösele, *Nanotechnology* **2008**, *44*, 335604.

[35] L. Liu, W. Lee, R. Scholz, E. Pippel, U. Gösele, *Angew. Chem. Int. Ed.* **2008**, *47*, 7004.